Breast Cancer Res Treat (2008) 109:417–426
DOI 10.1007/s10549-007-9671-z

REVIEW

Inflammatory breast cancer: PET/CT, MRI, mammography, and sonography findings

Wei T. Yang · Huong T. Le-Petross · Homer Macapinlac · Selin Carkaci · Ana M. Gonzalez-Angulo · Shaheenah Dawood · Erika Resetkova · Gabriel N. Hortobagyi · Massimo Cristofanilli

Received: 15 June 2007 / Accepted: 26 June 2007 / Published online: 26 July 2007

Abstract
Purpose To describe the role of Positron Emission Tomography/Computed Tomography (PET/CT), Magnetic Resonance Imaging (MRI), sonography, and mammography in patients with inflammatory breast cancer (IBC).
Materials and methods Patients who had been newly diagnosed with IBC and who had undergone mammography, sonography, MRI, PET/CT, or a combination of these were included in this study. The visibility of breast parenchymal lesion (BPLs), skin abnormalities, regional (axillary, supraclavicular, or internal mammary) nodal disease, and distant metastatic disease was documented with the imaging techniques.
Results Eighty patients (median age, 51 years, [range, 25–78 years]) were included in this study: 75 (94%) had undergone mammography, 76 (95%) sonography, 33 (41%) MRI, and 24 (30%) PET/CT. A primary BPL was found in 60 patients (80%) on mammography (mass or calcifications), 72 (95%) on sonography (mass or architectural distortion), 23 (96%) on PET/CT (hypermetabolic BPL), and 33 (100%) on MRI (enhancing BPL). Regional axillary nodal disease was found in 74 patients (93%) by histologic or cytologic examination, in 71 patients (93%) on sonography, in 21 (88%) on PET/CT, in 29 (88%) on MRI, and in 34 (45%) on mammography. Distant metastases in the bone, liver, and contralateral lymph nodes were diagnosed in nine patients (38%) on PET/CT.
Conclusion MRI was the most accurate imaging technique in detecting a primary BPL in IBC patients. Sonography can be useful in diagnosing regional nodal disease. PET/CT provides additional information on distant metastasis, and it should be considered in the initial staging of IBC.

Keywords Inflammatory breast cancer · PET/CT · MRI · Mammography · Sonography

W. T. Yang (✉) · H. T. Le-Petross · H. Macapinlac · S. Carkaci · A. M. Gonzalez-Angulo · S. Dawood · E. Resetkova · G. N. Hortobagyi · M. Cristofanilli
The University of Texas M. D. Anderson Cancer Center, 1515 Holcombe Blvd., Unit 1350, Houston, TX 77030, USA
e-mail: wyang@di.mdacc.tmc.edu

Introduction

Inflammatory breast cancer (IBC) is a rare, highly aggressive form of primary epithelial breast cancer that comprises 1–6% of breast cancer cases [1–3]. IBC is associated with a poor prognosis because of the likelihood that it has already micro-metastasized at diagnosis. Approximately 20% of patients with IBC have gross distant metastases at the time of diagnosis, and the mean 5-year overall survival rate in studies of IBC patients who have undergone current multidisciplinary therapy is between 20% and 40%, with a median survival duration of 12–36 months [1, 4, 5].

Clinically, IBC is characterized by the rapid onset of swelling and enlargement of the breast, ≤3 months typically elapsing from the first symptom or sign to diagnosis [4, 6]. The overlying skin remains intact, but there is erythema, often combined with "peau d'orange" texture, local tenderness, induration, and warmth. IBC can present with or without a palpable breast mass and is usually a poorly differentiated infiltrating ductal carcinoma. Histologic tissue diagnosis is problematic because it is difficult to define an area for biopsy.

Standard imaging findings using mammography and sonography have been previously described in IBC [7–13]. To the best of our knowledge, findings of IBC on magnetic

resonance imaging (MRI) and functional positron emission tomography/computed tomography (PET/CT) are scarce in the published literature [14–17]. In this retrospective study, we report the imaging findings using MRI, PET/CT, mammography, and sonography at the time of initial presentation in IBC patients.

Materials and methods

Patients

A database search was performed for patients newly diagnosed with IBC and evaluated at a single institution between January 2003 and January 2007. Patients who had undergone mammography, sonography, MRI, PET/CT, or a combination of these and had histopathologic review were included in this study. Images were reviewed by one of three imaging physicians (W.T.Y., H.T.L., H.M.) for this study, and the findings of BPLs, skin abnormalities, regional nodal disease, and distant metastatic disease were documented.

The clinical features of all patients including clinical presentation, clinical findings, and follow-up, were documented by one of three breast medical oncologists (A.G.A., S.D., M.C.). Histopathologic review was performed by one dedicated breast pathologist (E.R.). A waiver of informed consent was obtained, and the institutional review board approved this HIPAA-compliant study [18].

Mammography

Mammography was performed using a Lorad M3 mammography unit (Hologic, Inc., Boston, MA) or a General Electric Medical Systems DMR series unit (Milwaukee, WI). Standard two-view mammography was performed, with additional views as deemed necessary. One breast imager with 10 years' experience in breast imaging reviewed all available mammograms independently (W.T.Y.) with no knowledge of the clinical and other imaging findings. Breast parenchymal density was classified according to the American College of Radiology Breast Imaging Reporting and Data System (BIRADS) lexicon [19]. Mammograms were reviewed for focal masses; architectural distortion; asymmetric density; calcifications; and features associated with IBC such as trabecular distortion, skin thickening and retraction, and nipple retraction; and axillary lymphadenopathy. These were also classified according to the BIRADS lexicon [19]. PBLs were categorized as unifocal, multifocal, or multicentric.

Sonography

Real-time gray-scale and color Doppler sonography was performed using a Siemens Medical Solutions Elegra or Antares unit (Issaquah, WA) with a 5–13-MHz linear-array transducer. One of ten attending radiologists who specialized in breast sonography (range of experience, 5–10 years) had performed the sonographic examinations. The imager who interpreted the mammograms assessed the sonograms for masses (solid or cystic) and classified their shapes, margins, echo patterns, posterior acoustic features, and calcifications according to the BIRADS sonography lexicon [20]. The presence or absence of tumoral vascularity on color Doppler imaging was assessed and disease was classified as unilateral, bilateral, unifocal, multifocal, or multicentric in all patients who underwent US. Sonographic assessment of the regional lymph node basins, including the axillary, infraclavicular, internal mammary, and supraclavicular regions, is routinely performed in our institution and was documented according to previously published criteria [21–23].

MRI

MRI was performed with the patient lying prone in a General Electric 1.5-Tesla Signa EXCITE HD whole-body imaging system (General Electric Healthcare, Milwaukee, WI), that used a dedicated seven-channel breast coil (Invivo Corp., Orlando, FL). The imaging protocol included a precontrast axial T1-weighted SE (TR/TE 500/12) sequence; a sagittal, T2-weighted, fat-suppressed, FSE (TR/TE 6000/85 ms) sequence; dynamic, contrast-enhanced, sagittal, T1-weighted, three-dimensional (3D), fat-suppressed, FSPGR (TR/TE 18/4; flip angle, 15°, bandwidth 50) sequences, before and three times after the patient had been given an intravenous bolus injection of 0.1 mmol/l of gadopentetate dimeglumine (Magnevist, Berlex Laboratories, Berlin, Germany;) per kilogram body weight at 3 ml/s with an injector (Medrad Corp., Pittsburgh, PA); and delayed post-contrast, axial, T1-weighted, 3D, fat-suppressed, FSPGR sequence performed immediately after the dynamic series. The presence or absence of areas of abnormal enhancement was classified according to the BIRADS MRI lexicon by one breast imager with 5 years' experience in breast MRI (H.T.L.) [24]. Areas of abnormal enhancement were described as mass-like or non-mass-like, and enhancement kinetics, including initial and delayed phase patterns, was noted. Disease was categorized as unifocal, multifocal, or multicentric. Associated findings, including skin thickening and enhancement, axillary and internal mammary lymphadenopathy, and nipple and pectoralis muscle invasion, were also noted.

PET/CT

[^{18}F] Fluorodeoxyglucose (FDG) PET/CT imaging was performed using a General Electric Medical Systems Discovery ST camera (Waekusha, WI) in combination with the CT component from a General Electric CT product, the eight-slice Light-Speed Ultra [25, 26]. Patients were positioned supine in the PET/CT device with their arms raised upward. After fasting for at least 6 h, normal fasting blood glucose levels were determined to be <150 mg/dl for all patients. An intravenous injection of 370–555 MBq (10–15 mCi) of FDG was then given in the arm or central venous catheter opposite to the known cancer, and 2D emission scans were acquired at 3 min per FOV 60–90 min after FDG injection. PET images were reconstructed using standard vendor-provided reconstruction algorithms. Non-contrast-enhanced CT images were acquired in helical mode (speed, 13.5 mm/rotation) from the base of the skull to mid thigh during suspended mid-expiration at 3.75-mm slice thickness, 140 kVp, and 120 mA.

The CT, PET, and co-registered CT-PET images were reviewed in all standard planes along with maximum intensity whole body coronal projection images on a Xeleris workstation (General Electric Medical Systems) by a physician with 12 years' experience in evaluating PET images and 5 years experience in interpreting PET/CT images (H.M.). Images were reviewed to determine the presence of abnormal masses in the breast with or without FDG uptake, and associated skin changes. PBLs were categorized as unifocal, multifocal, or multicentric. Regional nodes were considered abnormal if the short axis diameter measured more than 1 cm. CT images were reviewed using lung, soft tissue, and bone windows. PET scans were analyzed visually and semi-quantitatively. FDG uptake was considered to be abnormal on visual analysis when uptake in the region of the primary tumor was substantially higher than the background uptake in the contralateral breast or axilla. The highest recorded FDG uptake was semiquantitatively analyzed, after being corrected for radioactive decay, according to the following formula: maximum standardized uptake value (SUV) = mean region of interest activity (mCi/ml)/injected dose (mCi)/body weight (g). The maximum SUVs in the primary breast and nodal lesions were obtained and an SUV of <2.0 was estimated as 2.0 for statistical analysis.

Histologic assessment

One dedicated breast pathologist (E.R.) reviewed the hematoxylin-and-eosin-stained slides of core biopsy, excisional biopsy, or mastectomy specimens to determine histologic tumor type, histologic grading, presence of angiolymphatic invasion, and presence or absence of dermal lymphatic invasion. Histologically, tumors were classified as invasive ductal carcinoma, invasive lobular carcinoma, invasive metaplastic carcinoma, ductal carcinoma in situ, or a combination of these types. Invasive tumors were graded on the basis of the Nottingham grading system (the Elston-Ellis modification of the Scarff-Bloom-Richardson system), which is a combined score based on an evaluation of tubule formation, mitotic count and nuclear pleomorphism, as described previously [27]. The use of axillary surgery, and the presence or absence of metastatic disease, were also documented. The presence of prognostic markers, including the overexpression of estrogen receptor (ER), progesterone receptor (PR), and HER-2/neu protein (as demonstrated by immunohistochemical analysis or by HER-2/neu oncogene amplification with fluorescent in situ hybridization), was recorded and interpreted as negative or positive on the basis of standard manufacturer recommendations.

Results

Eighty patients met the eligibility criteria. Their mean and median ages at the time of diagnosis were both 51 and 51 years (range, 25–78 years). The right breast was involved in 41 women (51%), and the left breast in 39 women (49%). All patients presented with breast erythema, skin edema, peau d'orange changes or a combination of these. Other clinical findings included palpable breast masses (30 patients [38]), breast swelling (22 [28%]), firmness (11 [14%]), and nipple retraction (2 [3%]). The remaining 15 patients (19%) had no associated clinical findings besides erythema. Most cancers were infiltrating ductal with or without associated ductal carcinoma in situ, high grade, and demonstrated and axillary nodal metastases (Table 1). Angiolymphatic and dermal lymphatic invasion were observed in slightly more than 50% of patients (Table 1). Thirty percent (24) of tumors were ER, PR, and Her-2/neu negative; 36% (29) were Her-2/neu positive; 35% (28) were ER positive; and 23% (18) were both ER and PR positive.

Seventy-five patients (94%) had mammography, 76 (95%) sonography, 33 (41%) MRI, and 24 (30%) had PET/CT (Tables 2–6). On mammography, 73 (97%) patients had non-fatty breasts (BIRADS parenchymal patterns 2, 3, or 4) and 60 (80%) patients had BPLs (mass, area of architectural distortion, asymmetry, or calcifications) (Table 2). Skin thickening was noted in 62 (83%) patients and trabecular distortion in 55 (73%) patients (Fig. 1). On sonography, BPLs (mass or architectural distortion) (Fig. 2) and skin thickening were each found in 95% of patients (72) (Table 3). MRI revealed malignant enhancing BPLs in all patients and skin thickening and enhancement

Table 1 Pathologic characteristics of IBC in 80 patients

Finding	Number of patients (%)
Pathologic diagnosis	
Infiltrating ductal carcinoma	32(40)
Infiltrating lobular carcinoma	2(3)
Mixed ductal/lobular carcinoma	4(5)
Metaplastic carcinoma	2(3)
Infiltrating ductal carcinoma + DCIS	32(40)
Infiltrating lobular carcinoma + DCIS	1(1)
Infiltrating ductal/lobular carcinoma + DCIS	1(1)
DCIS	3(4)
Unknown	3(4)
Nottingham grade	
1	2(3)
2	18(23)
3	57(71)
Unknown	3(4)
Angiolymphatic invasion	
Yes	41(51)
No	2(26)
Unknown	18(23)
Dermal lymphatic invasion	
Yes	46(58)
No	11(14)
Unknown	23(29)
Axillary lymph node metastases	
ALND performed	52(65)
Metastatic	33(41)
Metastatic by FNAB[a]	14(18)
Non-metastatic at ALND	5(6)
ALND not performed	
Metastatic by FNAB[b]	27(34)
Axillary node status unknown	1(1)
ER	
+	28(35)
–	51(64)
Unknown	1(1)
PR	
+	23(29)
–	56(70)
Unknown	1(1)
HER-2/neu	
+	29(36)
–	50(63)
Unknown	1(1)

Abbreviations: DCIS, ductal carcinoma in situ; ALND, axillary lymph node dissection; FNAB, fine needle aspiration biopsy; ER, estrogen receptor; PR, progesterone receptor.

[a] Negative at ALND after neoadjuvant chemotherapy

[b] ALND was not performed because the patient had known metastases or was still undergoing neoadjuvant chemotherapy

Table 2 Mammography findings of IBC in 75 patients

Finding	Number of patients (%)
Breast parenchymal density BIRADS	
1	2(3)
2	26(35)
3	43(57)
4	4(5)
Primary breast parenchymal lesion[a]	60(80)
Mass	24(32)
Architectural distortion	12(16)
Focal asymmetry	4(5)
Global asymmetry	4(5)
Calcifications	
Yes	31(41)
No	44(59)
Disease extent	
Unifocal	35(47)
Multifocal	10(13)
Multicentric	15(20)
None	15(20)
Trabecular distortion	
Yes	55(73)
No	20(27)
Skin thickening	
Yes	62(83)
No	13(17)
Associated findings	
Nipple retraction	7(9)
Axillary adenopathy	34(45)

Abbreviations: BIRADS, Breast Imaging Reporting and Data System

[a] Some patients had more than one finding

in 94% of patients (31) (Table 4) (Fig. 3). PET/CT demonstrated both hypermetabolic BPLs and skin thickening in 96% of patients (23) (Table 5) (Fig. 4). One case was false-negative on PET/CT, negative on mammography, and showed diffuse architectural distortion on sonography. MRI was not performed in this patient. The pathology for this patient was intralymphatic carcinoma within dermis and breast parenchyma. Of the 15 false-negative cases on mammography, sonography showed a mass or architectural distortion in 12, and was also false-negative in 3.

The percentage of women diagnosed with multifocal and multicentric disease was higher with sonography (62%), MRI (82%), and PET/CT (71%) than with mammography (33%). A primary BPL on mammography was most frequently a mass, area of architectural distortion, focal or global asymmetry (58%). Calcifications were present in 41% of patients on mammography. Sonography demonstrated a mass or architectural distortion in 95% of patients with associated global skin and subcutaneous

Table 3 Ultrasound findings of inflammatory breast cancer in 76 patients

Finding	Number of patients (%)
Primary breast parenchymal lesion	
Mass	54(71)
Architectural distortion	18(24)
None of the above	4(5)
Disease extent	
Unifocal	25(33)
Multifocal	19(25)
Multicentric	28(37)
None	4(5)
Color Doppler Vascularity	
Yes	56(74)
No	10(13)
Not done	10(13)
Skin thickening	
Yes	72(95)
No	4(5)
Regional adenopathy	
Axillary	71(93)
Infraclavicular	38(50)
Internal mammary	10(13)
Supraclavicular	25(33)

Table 4 MRI findings of IBC in 33 patients

Finding	Number of patients (%)
Primary breast parenchymal lesion	
Enhancement mass-like	23(70)
Enhancement non-mass-like	10(31)
Disease extent	
Unifocal	6(18)
Multifocal	3(9)
Multicentric	24(73)
Skin thickening	
Yes	32(97)
No	1(3)
Skin enhancement	
Yes	31(94)
No	2(6)
Regional adenopathy	
Axillary	29(88)
Internal mammary	5(15)
Associated findings	
Architectural distortion	20(61)
Nipple retraction	5(15)
Skin retraction	4(12)
Edema	18(54)
Pectoralis invasion	2(6)
Chest wall	1(3)

thickening and dilated lymphatics. An unusual sonographic feature of IBC which to the best of our knowledge has not been described in the literature was a "linear infiltrative hypoechogenicity" dissecting through the breast parenchyma resulting in loss of normal architecture that was best demonstrated on extended-field-of-view US imaging (Fig. 5). MRI showed a primary BPL as a heterogeneously enhancing mass or non-mass-like area of enhancement in all patients, frequently associated with skin thickening and enhancement. The most frequent MRI findings in our study were multiple masses with irregular margins and heterogeneous internal enhancement (Fig. 3). Kinetic evaluation of the index breast lesion demonstrated initial rapid enhancement with washout or plateau curves in 97% of the patients. A primary BPL on PET/CT was a hypermetabolic breast lesion with associated hypermetabolic skin thickening (96% of patients) frequently in a multifocal or multicentric distribution (Fig. 4).

Regional axillary nodal disease was diagnosed in 93% of all patients (74) by pathology, 93% (71) of patients on sonography, 88% (21) of patients on PET/CT, 88% (29) of patients on MRI, and 45% (34) of patients on mammography. Supraclavicular, infraclavicular, or internal mammary (N3) nodal disease was diagnosed in at least 50% of patients on sonography and 25% on PET/CT. Distant metastases in the bone, liver, and contralateral lymph nodes were found in 38% of patients (9) on PET/CT (Table 5) (Fig. 4); in all of these patients, metastases were confirmed by either histology (44%) or ancillary correlative imaging (56%) (Table 6). Four patients underwent biopsy of contralateral supraclavicular lymph node ($n = 2$), contralateral axillary node ($n = 1$), and liver ($n = 1$). The remaining five patients underwent MRI of the thoracic spine [$n = 2$], MRI of the lumbar spine [$n = 1$], CT of the liver [$n = 2$], CT of the pelvis [$n = 1$], CT of the thorax [$n = 1$], or whole body bone imaging [$n = 1$] (Table 6).

The comparative accuracy of mammography, sonography, MRI and PET/CT in diagnosing primary BPLs, multicentric or multifocal disease, axillary nodal disease and distant metastases (PET/CT only) is described in Table 7.

Discussion

A primary BPL was found in all IBC cases ($n = 33$) on MRI, 96% ($n = 24$) on PET/CT, 95% ($n = 76$) on sonography, and 80% ($n = 75$) on mammography. In addition, mammography was the least sensitive imaging method for diagnosing multifocal and multicentric disease. These findings suggest that mammography is not the most

Table 5 PET/CT findings of IBC in 24 patients

Finding	Number of patients (%)
Primary hypermetabolic breast lesion	
Yes	23(96)
No	1(4)
Disease extent	
Unifocal	6(25)
Multifocal	2(8)
Multicentric	15(63)
None	1(4)
Hypermetabolic skin thickening	
Yes	23(96)
No	1(4)
Regional adenopathy	
Yes[a]	22(92)
Axillary	21(88)
Subpectoral	4(17)
Internal mammary	6(25)
Supraclavicular	3(13)
No	2(8)
Distant metastasis	
Yes	9(38)
No	15(63)

[a] This number includes patients who had axillary, subpectoral, internal mammary, or supraclavicular lymphadenopathy. Some patients had more than one nodal disease site

valuable initial imaging modality for women with IBC. Ninety-seven percent of women in this study had non-fatty breasts despite a median age of 51 years. This observation has not been previously reported for women with IBC to the best of our knowledge. We postulate that this dense breast parenchymal background may have contributed in part to the poor visibility of a primary BPL on mammography in 15 (20%) patients, and may also reflect an underlying risk factor for this disease [28, 29].

Table 6 Distant metastatic disease diagnosed by PET/CT in nine patients and confirmed by histologic examination or ancillary imaging

Patient	Site of metastasis	Max SUV	Biopsy	Correlative imaging
1	Contralateral SCN	9.2	Yes	CT thorax
2	Thoracic VB	5.9	No	MRI thoracic spine
3	Liver	7.7	No	CT liver (4 cm)
	Proximal right femur	6.7	No	CT follow up
4	Contralateral SCN	6.2	No	CT thorax
5	Contralateral SCN	4.2	Yes	CT thorax
6	Liver	3.1	Yes	CT liver
	Pelvic skeleton	4.5	No	CT pelvis, Bone scan
7	Contralateral AXN	3.3	Yes	CT thorax
8	Liver, left lobe	9.0	No	CT (6 cm bilobed)
	Liver, right lobe	5.3	No	CT (6 cm bilobed)
9	Thoracic VB	7.7	No	MRI thoracic spine
	Lumbar VB	6.5	No	MRI lumbar spine

Abbreviations: AXN, axillary node; SCN, supraclavicular node; Max SUV, maximum standardized uptake value; VB, vertebral body

Regional axillary nodal disease was found in 88%, 88%, and 93% of cases on MRI, PET/CT, and sonography, respectively. Supraclavicular, infraclavicular, or internal mammary nodal disease was diagnosed in at least 50% of patients on sonography and 25% on PET/CT. Pre-treatment nodal staging using both sonography and PET/CT may affect locoregional therapeutic planning, which is based on initial disease involvement. In previously reported series, axillary adenopathy has been found in 22–56% of IBC cases (mean, 28%) [1, 3, 4]. In our study, we found an unusually high percentage of axillary nodal involvement (93%).

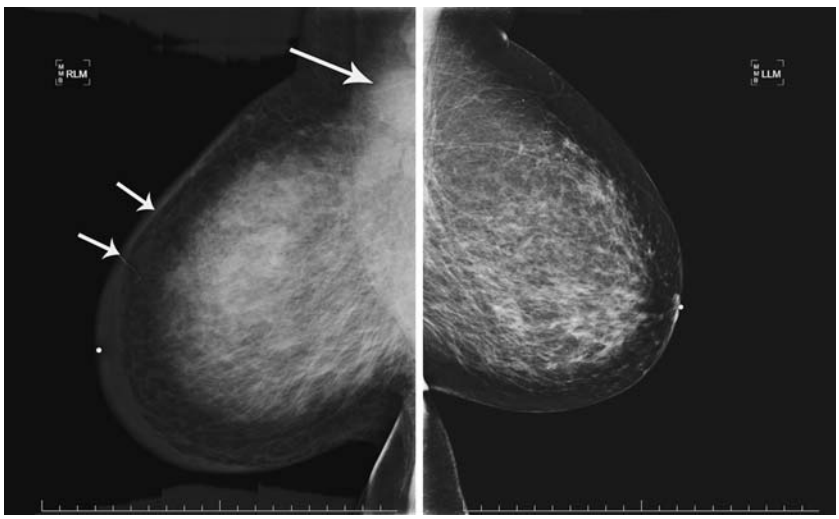

Fig. 1 Bilateral mediolateral oblique mammograms in a 54-year-old female show global skin and trabecular thickening (short arrows) of the right breast with associated right axillary adenopathy (long arrow). No visible primary breast parenchymal lesion is noted in the right breast

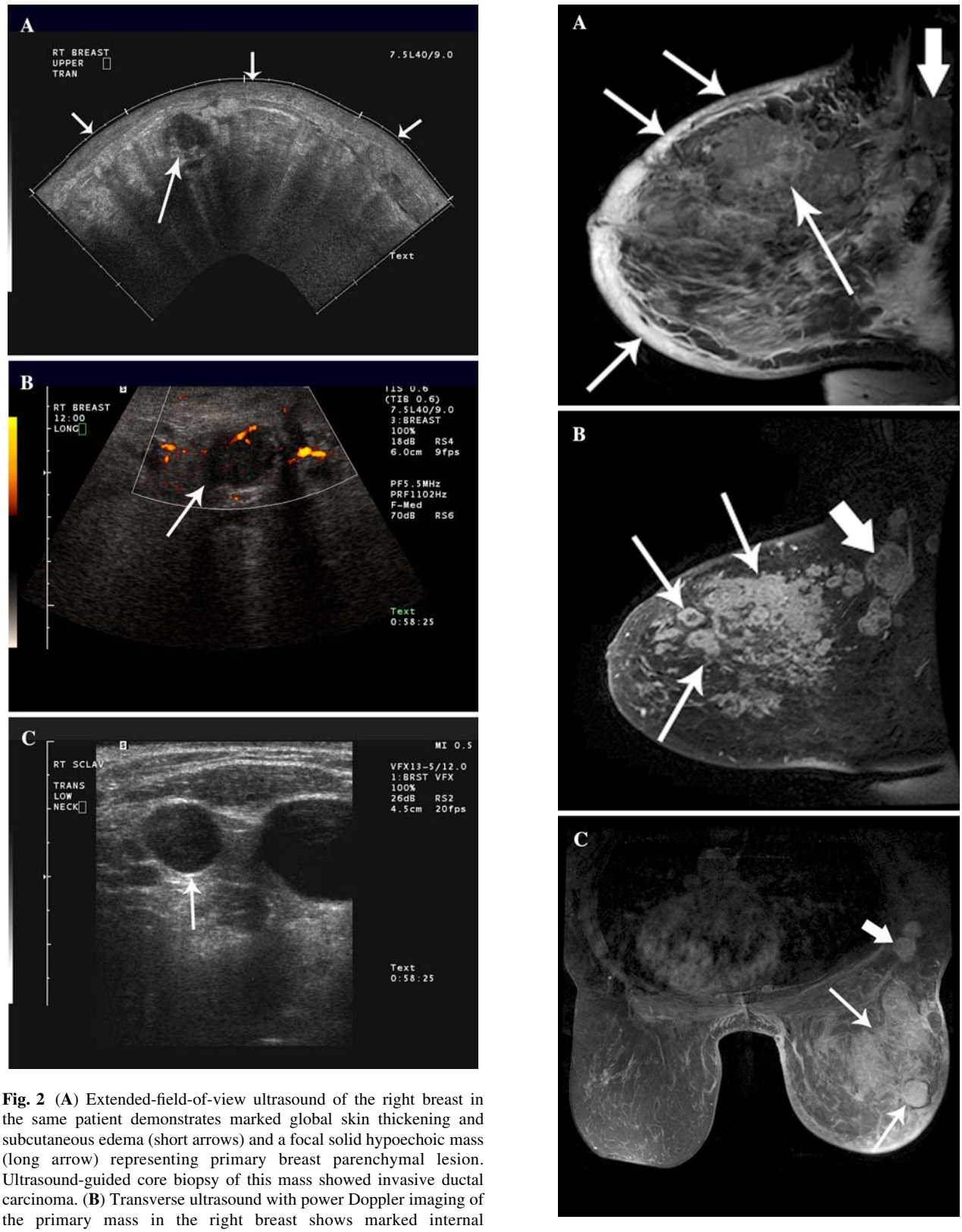

Fig. 2 (**A**) Extended-field-of-view ultrasound of the right breast in the same patient demonstrates marked global skin thickening and subcutaneous edema (short arrows) and a focal solid hypoechoic mass (long arrow) representing primary breast parenchymal lesion. Ultrasound-guided core biopsy of this mass showed invasive ductal carcinoma. (**B**) Transverse ultrasound with power Doppler imaging of the primary mass in the right breast shows marked internal hypervascularity. (**C**) Transverse ultrasound of the right supraclavicular region shows a solid hypoechoic node that showed metastatic carcinoma on ultrasound-guided fine needle aspiration biopsy

◀ **Fig. 3** (**A**) Sagittal T2-weighted fast spin-echo image with fat suppression shows a dominant heterogeneous mass in the superior right breast (long arrow), global skin and subcutaneous edema (medium arrows), and right axillary adenopathy (broad arrow). (**B**) Sagittal fat suppressed 3D spoiled gradient-recalled-echo sequence with parallel imaging at 2 min post-contrast administration demonstrates multiple rim enhancing tumor masses (arrows) in the right breast and malignant-appearing necrotic right axillary lymph nodes (broad arrow). (**C**) Delayed axial fat suppressed contrast-enhanced 3D fast spoiled gradient-recalled echo MR image reveals multiple heterogeneously enhancing masses in the central and lateral right breast (arrows), and right axillary adenopathy (broad arrow)

Metastatic disease was diagnosed in 38% of patients on PET/CT and was confirmed in all these patients either by histologic examination (44%) or ancillary correlative imaging (56%). This rate of metastatic disease is higher than that reported for breast cancers in general, and may reflect the aggressive nature of IBC. These findings suggest that despite the cost, PET/CT should be considered in the initial staging of women diagnosed with IBC. The cost of a PET/CT study is $2,567.57 according to the Medicare fee schedule for Harris County, TX. This compares with $399.53 for CT of the thorax with contrast, $407.62 for CT of the abdomen with contrast, and $387.42 for CT of the pelvis with contrast, according to the Medicare fee schedule for Harris County, TX. The cost of whole body bone imaging is relatively low, $203.42, according to the Medicare fee schedule for Harris County, TX. Finally, the cost of MRI of the spine is high (C spine with contrast, $1,024.10, T spine with contrast, $1,007.69, L spine with contrast, $1,024.10, according to the Medicare fee schedule for Harris County, TX).

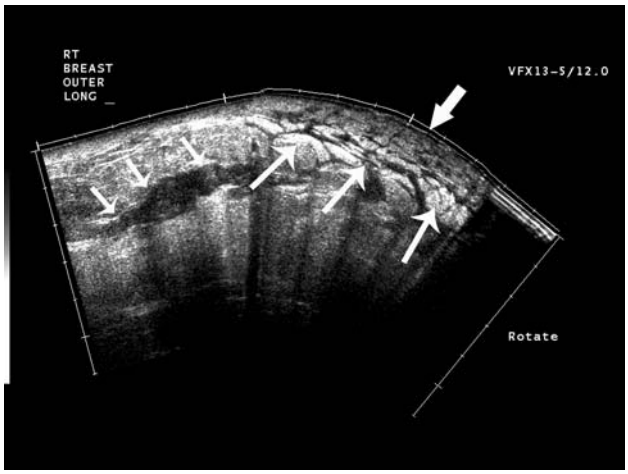

Fig. 5 Extended-field-of-view ultrasound of the right breast in the same patient demonstrates marked global skin thickening (broad arrow), subcutaneous edema (medium arrows) and linear dissection through the breast parenchyma (short arrows) representing primary breast parenchymal lesion

The differential diagnosis of IBC is non-puerperal mastitis, locally advanced breast cancer, and primary breast

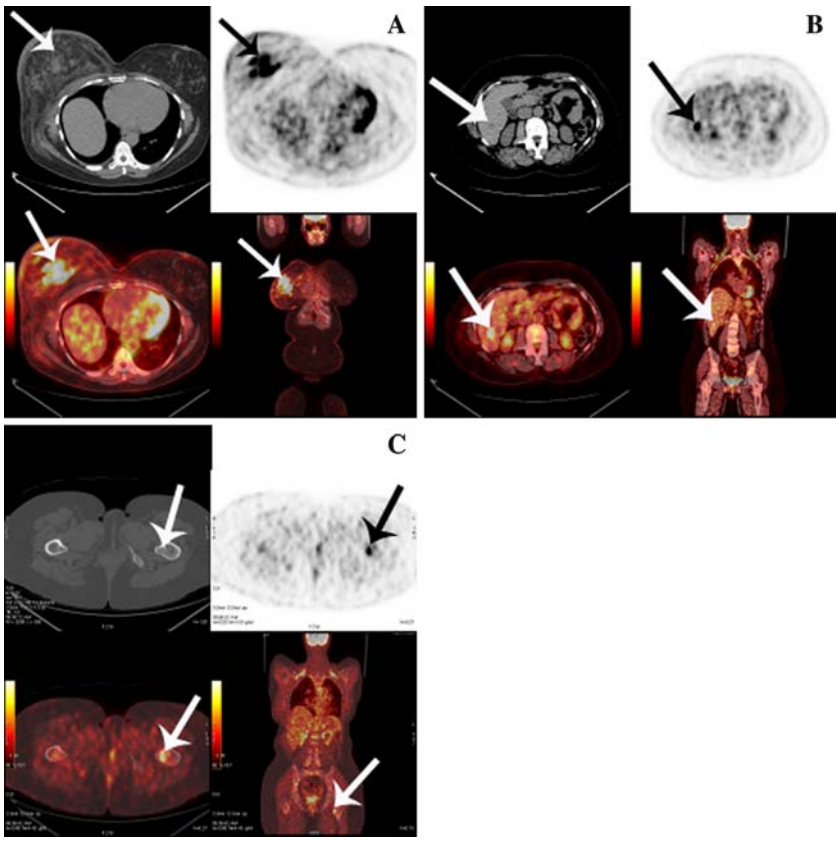

Fig. 4 (**A**) PET/CT shows multicentric hypermetabolism in the right breast (arrow) associated with hypermetabolic diffuse skin thickening. (**B**) PET/CT shows a solitary focal hypermetabolic focus in the right lobe of the liver (arrows) that showed a maximum SUV of 5.7. Corresponding CT of the liver shows a focal hypoechoic mass with indistinct margins. (**C**) PET/CT shows a solitary focal hypermetabolic focus in the left proximal femur (arrows) that showed a maximum SUV of 7.7. Corresponding CT of the proximal femur shows this area of hypermetabolism to be within the marrow (whole body bone imaging was negative in this patient)

Table 7 Comparison of mammography, sonography, MRI, and PET/CT in diagnosing breast parenchymal lesions, multicentric/multifocal disease, axillary metastases, and distant metastases (PET/CT only)

	Breast parenchymal lesions					Axillary metastases				Distant metastases			
	SN (%)	SP	NPV	PPV	MD (%)	SN (%)	SP (%)	NPV (%)	PPV (%)	SN (%)	SP (%)	NPV (%)	PPV (%)
M (n = 75)	80	N/A	N/A	N/A	33	48	100	90	100	N/A	N/A	N/A	N/A
S (n = 76)	95	N/A	N/A	N/A	62	100	100	100	100	N/A	N/A	N/A	N/A
MRI (n = 33)	100	N/A	N/A	N/A	82	91	100	75	100	N/A	N/A	N/A	N/A
PET/CT (n = 24)	96	N/A	N/A	N/A	71	95	100	33	100	100	93	100	90

Abbreviations: M, mammography; MD, multifocal or multicentric breast disease; N/A, not applicable; NPV, negative predictive value; PPV, positive predictive value; S, sonography; SN, sensitivity; SP, specificity

lymphoma, all of which may result in skin thickening, diffuse breast enlargement, and increased mammographic density. The differential diagnosis between IBC and locally advanced breast cancer should be excluded based on clinical history [14, 30, 31] and is necessary to avoid data contamination.

The imaging findings of IBC in our study concur with those of previous studies [7–14]. Diffusely increased parenchymal density (now termed global asymmetry according to the ACR BIRADS lexicon [19]), trabecular distortion, and skin thickening were noted on mammography. A primary mammographic abnormality including a mass, architectural distortion, asymmetry, or calcifications was less common, and may reflect the overall increased breast density that masks the infiltrative mature of the underlying tumor. The presence of a BPL seems to be the most variable and elusive finding, with an incidence of 15–96% (mean, 38%) in previous studies [7–10].

Sonography has been useful in localizing primary BPLs to facilitate biopsy and for evaluation of the regional nodes [9, 11, 13, 15]. In our study, primary BPLs were more frequently visible on sonography than on mammography. An interesting sonographic feature best demonstrated on extended-FOV imaging comprised a linear infiltrative pattern that dissected through the breast parenchyma with loss of normal architecture. Targeting this area of focal linear infiltration in the absence of a discrete mass on sonography yielded a diagnosis of cancer and enabled evaluation of biologic markers in our study.

A few studies have described the MRI features of IBC as skin thickening and enhancement [14–16]. Chow et al. reported that the affected breast was deformed and enlarged, and the most frequent observation was an infiltrative mass represented by a "reticular/dendritic pattern" of enhancement [14]. The most frequent MRI findings in our study were multiple masses with irregular margins and heterogeneous internal enhancement associated with a washout or plateau kinetic curve in 97% of patients.

A single PET study of seven patients with IBC demonstrated diffusely increased or intense foci of increased uptake in enlarged breasts with increased skin uptake [17]. PET/CT is an emerging imaging method that is widely gaining clinical acceptance because of its ability to co-register both anatomic and functional information on one image [32]. To our knowledge, ours is the first study of PET/CT in IBC showing that PET/CT is accurate at demonstrating loco-regional disease and distant metastases.

A limitation of this retrospective review is that not all patients were assessed with all four imaging modalities. However, this reflects true clinical practice and the status of health care over the past decade, where women with breast cancer frequently commence therapy without having a complete imaging workup. The disease biology of IBC which is a rare, aggressive and frequently lethal cancer that often requires prompt treatment due to the galloping pace of disease progression observed without institution of treatment also contribute to the lack of multimodality imaging in all patients. Finally, the retrospective nature of this study captures the evolution of diagnostic imaging practice where emerging imaging modalities, namely MRI and PET/CT, are gradually gaining clinical acceptance and approval. The preliminary findings in our single institution study suggest that MRI would be the preferred initial imaging modality for IBC and that PET/CT would be an excellent companion for detection of distant metastases.

References

1. Levine PH, Steinhorn SC, Ries LG, Aron JL (1985) Inflammatory breast cancer: the experience of the surveillance, epidemiology, and end results (SEER) program. J Natl Cancer Inst 74:291–297
2. Chang S, Parker SL, Pham T, Buzdar AU, Hursting SD (1998) Inflammatory breast carcinoma incidence and survival: the surveillance, epidemiology, and end results program of the National Cancer Institute, 1975-1992. Cancer 82:2366–2372
3. Hance KW, Anderson WF, Devesa SS, Young HA, Levine PH (2005) Trends in inflammatory breast carcinoma incidence and survival: the surveillance, epidemiology, and end results program at the National Cancer Institute. J Natl Cancer Inst 97:966–975
4. Lee B, Tannenbaum N (1924) Inflammatory carcinoma of the breast: a report of twenty-eight cases from the breast clinic of memorial hospital. Surg Gynecol Obstet 39:580–585
5. Jaiyesimi IA, Buzdar AU, Hortobagyi G (1992) Inflammatory breast cancer: a review. J Clin Oncol 10:1014–1024

6. Dirix LY, Dam PV, Prove A et al (2006) Inflammatory breast cancer: current understanding. Curr Opin Oncol 18:563–571
7. Dershaw DD, Moore MP, Liberman L et al (1994) Inflammatory breast carcinoma: mammographic findings. Radiology 190:831–834
8. Droulias CA, Sewell CW, McSweeney MB et al (1976) Inflammatory carcinoma of the breast: a correlation of clinical, radiologic and pathologic findings. Ann Surg 184:217–222
9. Gunhan-Bilgen I, Ustun EE, Memis A (2002) Inflammatory breast carcinoma: mammographic, ultrasonographic, clinical, and pathologic findings in 142 cases. Radiology 223:829–838
10. Kushwaha AC, Whitman GJ, Stelling CB et al (2000) Primary inflammatory carcinoma of the breast: retrospective review of mammographic findings. AJR Am J Roentgenol 174:535–538
11. Caumo F, Gaioni MB, Bonetti F et al (2005) Occult inflammatory breast cancer: review of clinical, mammographic, US and pathologic signs. Radiol Med (Torino) 109:308–320
12. Tardivon AA, Viala J, CorvellecRudelli A et al (1997) Mammographic patterns of inflammatory breast carcinoma: a retrospective study of 92 cases. Eur J Radiol 24:124–130
13. Lee KW, Chung SY, Yang I et al (2005) Inflammatory breast cancer: imaging findings. Clin Imaging 29:22–25
14. Chow CK (2005) Imaging in inflammatory breast carcinoma. Breast Dis 22:45–54
15. Belli P, Costantini M, Romani M et al (2002) Role of magnetic resonance imaging in inflammatory carcinoma of the breast. Rays 27:299–305
16. Rieber A, Tomczak RJ, Mergo PJ et al (1997) MRI of the breast in the differential diagnosis of mastitis versus inflammatory carcinoma and follow-up. J Comput Assist Tomogr 21:128–132
17. Baslaim MM, Bakheet SM, Bakheet R et al (2003) 18-Fluorodeoxyglucose-positron emission tomography in inflammatory breast cancer. World J Surg 27:1099–1104
18. Johnson MS, Gonzales MN, Bizila S (2005) Responsible conduct of Radiology research. Part V. The Health Insurance Portability and Accountability Act and Research. Radiology 237:757–764
19. American College of Radiology (ACR) (2003) ACR BI-RADS – Mammography. In ACR breast imaging reporting and data system, breast imaging atlas. American College of Radiology, Reston, VA
20. American College of Radiology (ACR). (2003) ACR BI-RADS – Ultrasound. In ACR breast imaging reporting and data system, breast imaging atlas. American College of Radiology, Reston, VA
21. Yang WT, Ahuja A, Tang A, Suen M, King W, Metreweli C (1996) High resolution sonographic detection of axillary lymph node metastases in breast cancer. J Ultrasound Med 16:241–246
22. Vlastos G, Fornage BD, Mirza NQ et al (2000) The correlation of axillary ultrasonography with histologic breast cancer downstaging after induction chemotherap. Am J Surg 179:446–452
23. Scatarige JC, Hamper UM, Sheth S, Allen HA III (1989) Parasternal sonography of the internal mammary vessels: technique, normal anatomy, and lymphadenopathy. Radiology 172:453–457
24. American College of Radiology (ACR) (2003) ACR BI-RADS – Magnetic Resonance Imaging. In ACR breast imaging reporting and data system, breast imaging atlas. American College of Radiology, Reston, VA
25. Mawlawi O, Podoloff DA, Kohlmyer S et al (2004) Performance characteristics of a newly developed PET/CT scanner using NEMA standards in 2D and 3D modes. J Nucl Med 45:1734–1742
26. Mawlawi O, Podoloff D, Macapinlac H (2003) Evaluation of clinical image quality and lesion detectability of the GE Discovery ST (DST) PET/CT scanner. J Nucl Med 44:Supplement 282 p
27. Elston CW, Ellis IO (1998) Assessment of histologic grade. In: Elston CW, Ellis IO (eds) The breast, vol 13. Churchill Livingstone, Edinburgh, New York, pp 356–384
28. Boyd NF, Byng JW, Jong RA et al (1995) Quantitative classification of mammographic densities and breast cancer risk: results from the Canadian National Breast Screening Study. J Natl Cancer Inst 87:670–675
29. Harvey JA, Bovbjerg VE (2004) Quantitative assessment of mammographic breast density: relationship with breast cancer risk. Radiology 230:29–41
30. Anderson WF, Chu KC, Chang S (2003) Inflammatory breast carcinoma and noninflammatory locally advanced breast carcinoma: distinct clinicopathologic entities? J Clin Oncol 21:2254–2259
31. Walshe JM, Swain SM (2005) Clinical aspects of inflammatory breast cancer. Breast Dis 22:35–44
32. Fueger BJ, Weber WA, Quon A et al (2005) Performance of 2-Deoxy-2-[F-18]fluoro-D-glucose Positron Emission Tomography and Integrated PET/CT in restaged breast cancer patients. Mol Imaging Biol 7:369–376